Hindawi
International Journal of Energy Research
Volume 2023, Article ID 2072245, 11 pages
https://doi.org/10.1155/2023/2072245

Research Article

Comparative Study of Ba, Cs, K, and Li as Promoters for Ru/$La_2Ce_2O_7$-Based Catalyst for Ammonia Synthesis

Hizkia Manuel Vieri,[1,2] **Arash Badakhsh**,[1,3] **and Sun Hee Choi**[1,2]

[1]*Hydrogen·Fuel Cell Research Center, Korea Institute of Science and Technology (KIST), Seoul 02792, Republic of Korea*
[2]*Energy & Environment Technology, KIST School, University of Science and Technology (UST), Seoul 02792, Republic of Korea*
[3]*PNDC, University of Strathclyde, Glasgow G68 0EF, UK*

Correspondence should be addressed to Sun Hee Choi; shchoi@kist.re.kr

Received 15 November 2022; Revised 5 April 2023; Accepted 2 May 2023; Published 13 May 2023

Academic Editor: Sanjay Basumatary

Ammonia is one of the promising carriers for hydrogen and a critical ingredient in many industries including fertilizers and pharmaceuticals. In the KAAP process, ruthenium- (Ru-) based catalysts showed 10-20 more activity compared with iron- (Fe-) based catalysts. The modifications that are applied to Ru-based catalysts revolve around changing the material of its support and/or promoters. This study compares the performance of a Ru-based catalyst for ammonia synthesis supported by $La_2Ce_2O_7$ using barium (Ba), cesium (Cs), potassium (K), and lithium (Li) as promoters. Based on structural, physicochemical, adsorption, and electronic state analysis, the Cs-promoted catalyst is expected to perform best among all the promoted catalysts, while our findings suggest that the K-promoted catalyst performed the best in the actual catalytic reaction. This result will affect the development of Ru/$La_2Ce_2O_7$-based catalysts, especially in ammonia synthesis at different temperatures and pressures.

1. Introduction

Hydrogen (H_2) is one of the most promising energy storage materials. However, the low density of H_2 makes its transport difficult. The conversion of hydrogen to ammonia (NH_3) is a promising solution for its easy transportation. Hydrogen is first produced by water electrolysis and then reacted with nitrogen to form ammonia. After being transported, ammonia is dehydrogenated back into hydrogen and nitrogen [1]. The Haber-Bosch process is most commonly used in the industry to produce ammonia with the help of an iron- (Fe-) based catalyst [2]. The drawback of this process is that the strong bonding energy of the nitrogen triple bond requires very high temperatures and pressures to obtain high ammonia yields (>450°C and >20 MPa) [3]. In 1972, Aika et al. pioneered the use of a Ru catalyst for ammonia synthesis, which showed high activity under mild conditions (600 Torr pressure and 350°C temperature) [4].

Various catalyst supports have also been coupled with Ru. Ru/$La_2Ce_2O_7$ (Ru/LCO) catalysts have been reported to be stable and easy to synthesize. Additionally, they have higher catalytic activity than other established catalysts such as Cs^+/Ru/MgO and Ba^{2+}/Ru/activated carbon [5]. The addition of Ce can act as a nest to form strong interactions between transition metals (Ru) and Ce through strong metal-support interaction (SMSI), increasing the number of donated electrons and reducing the water vapor content [6–8]. During ammonia synthesis, Ru catalysts can be inhibited by H_2. The addition of La to a Ru catalyst supported by zeolite significantly eliminates H_2 inhibition or poisoning [9]. The donated electrons can easily break the N_2 triple bonds.

Promoters are used for further enhancing the catalytic activity. They can be classified into structural and electronic promoters [10]. Considerable research has already been conducted on using alkali metal, alkali earth metal, and rare earth metal as promoters for the catalysts used in ammonia synthesis [11]. In addition to being commonly used as promoters, alkali metals are recognized for their ability to improve the activity, selectivity, and stability of heterogeneous catalysts in many important chemical processes [12].

K and Cs can increase the chemisorption ability of the Ru surface, while Li can facilitate nondissociative ammonia synthesis [13–15]. The influence of Ba on increasing the electron-donating ability of Ru has also been reported [3].

The donation of electrons to the Ru surface by alkali metals under the H_2 atmosphere can facilitate the adsorption of N_2 by promoting the donation of electron density from Ru to the π^* antibonding orbital of N_2 [4, 16–18]. In an experiment employing Ru/Ba/$La_{1.75}Ce_{1.75}O_3$ and Ru/ZrH_2, Ba acted as an electronic promoter [3, 19]. Conversely, other studies on Ru/MgO and Ru/Si_3N_4 showed that Ba acted as a structural promoter rather than an electronic promoter [20, 21]. Additionally, Gao et al. reported the role of Ba as a structural promoter [12]. Therefore, we report a comparative study of Li, K, Cs, and Ba as promoters for Ru/$La_2C_2O_7$-supported catalysts. The order of electronegativity of the promoters is Li > Ba > K > Cs. In this study, the order of the activity ranks was obtained as Cs > K > Ba > Li, which is different from the ranks reported by Raróg et al. [22] and Forni et al. [23].

The optimum amounts of Ba, Cs, K, Li, and Li-Ba have been reported to be 7 wt%, 4 wt%, 10 wt%, 7.6 wt%, and 12 wt% (5 wt% Ba, 7.6 wt% Li), respectively [3, 15, 24, 25]. However, a comparative study of promoters generally utilizes the same amount of each [19]. Therefore, in this study, 4 wt% of each promoter was used. The promoter addition can be performed before or after Ru impregnation into the support [3, 13, 25, 26]. Previous work has shown that exsolved Ru on $BaCe_xO_y$ catalysts prepared using a high-intensity ball milling method exhibit greater durability than the catalysts prepared in this study. However, given the fact that impregnated Ru on $BaCe_xO_y$ still has greater catalytic activity and metal dispersion, we choose to use the traditional wet-impregnation method to prepare our catalyst [27]. In this study, we will add that after Ru impregnation. The promoter composition also needs to be optimized to understand its interaction not only with Ru but also with the support. We focused on the impact of promoter type and composition on the morphological and chemical characteristics over the promoted Ru/LCO, which were thoroughly characterized using X-ray diffraction (XRD), CO chemisorption, temperature-programmed reduction/desorption (TPR/TPD), Brunauer-Emmett-Teller (BET), X-ray photoelectron spectroscopy (XPS), and transmission electron spectroscopy (TEM).

2. Methods

2.1. Preparation of Catalysts. $Ru_3(CO)_{12}$ was used as the Ru precursor, owing to its stronger metal-support interactions than other precursors [28]. A stoichiometric amount of $La(NO_3)\cdot 6H_2O$ (99.999%, Sigma-Aldrich) and $Ce(NO_3)\cdot 6H_2O$ (99%, Sigma-Aldrich) were dissolved in a 3 M ammonia solution (Junsei) and coprecipitated for 12 h to make $La_2Ce_2O_7$. The precipitated sample was filtered with distilled water to remove the ammonia solution. The filtered samples were then mixed with various promoters. CeO_2 and La_2O_3 were also made with a similar method to compare their structure with $La_2Ce_2O_7$ perovskite. Additionally, CeO_2 and La_2O_3 powder were also mixed to form CeO_2-La_2O_3 composite oxide.

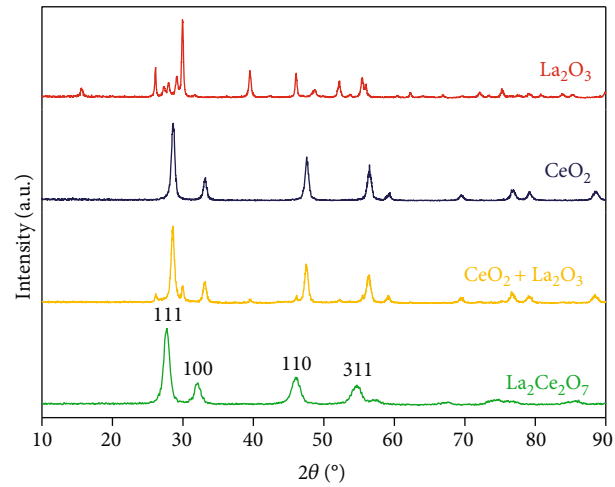

Figure 1: X-ray diffraction patterns of the promoted Ru/LCO catalysts.

For the Ba^{2+}-promoted catalyst, $Ba(OH)_2$ powder was added to the filtered sample to obtain a specific amount of barium. Subsequently, the mixtures of promoter and support were dried in an oven at 80°C for 12 h and then calcined at a ramping rate of 5°C/min using a muffle oven for 5 h at 700°C. The resulting powder was impregnated with $Ru_3(CO)_{12}$ to obtain 5 wt% Ru. Ru/K/LCO, Ru/Li/LCO, and Ru/Cs/LCO were prepared by adding the corresponding precursors, as described for the Ru/Ba/LCO catalyst. KOH, LiOH, and $CsCO_3$ powders were added to the filtered samples to obtain 4 wt% lithium, 4 wt% potassium, and 4 wt% cesium for the K^+-promoted and Cs^+-promoted catalysts, respectively.

CeO_2 and La_2O_3 were also made with a similar method to compare their structure with $La_2Ce_2O_7$ perovskite.

2.2. NH_3 Synthesis. Before testing, the catalyst samples were reduced in a tubular furnace under 10% H_2/Ar gas at 450°C for 1 h. The reducing time was set based on the experiment done by Ogura et al. [5], and the temperature was set by our optimization (Figure S1). Subsequently, 100 mg of the sample was placed inside a tubular reactor (ID: 3/8″) and packed with quartz wool and Al_2O_3 beads ($d = 2$ mm). The reaction was performed first at 1 MPa constant pressure in the temperature range of 300–400°C and then at 400°C constant temperature with pressures of 0, 0.1, 0.3, 0.5, and 1 MPa. The reactor was filled with 25% N_2/75% H_2 gas at a flow rate of 90 NmL. The NH_3 synthesis rate was determined using the titration method, with the effluent gas flowing into a 0.1 M H_2SO_4 solution (95–98%, Sigma-Aldrich). The change in the solution conductivity (Orion Star™ A212 conductivity benchtop meter) indicated the ammonia synthesis rate. The detail of the NH_3 synthesis rate calculation is explained in Figures S22–S23. NH_3 synthesis experiments were conducted using a gas mixture of 25% N_2 and 75% H_2 flow rate to prevent the

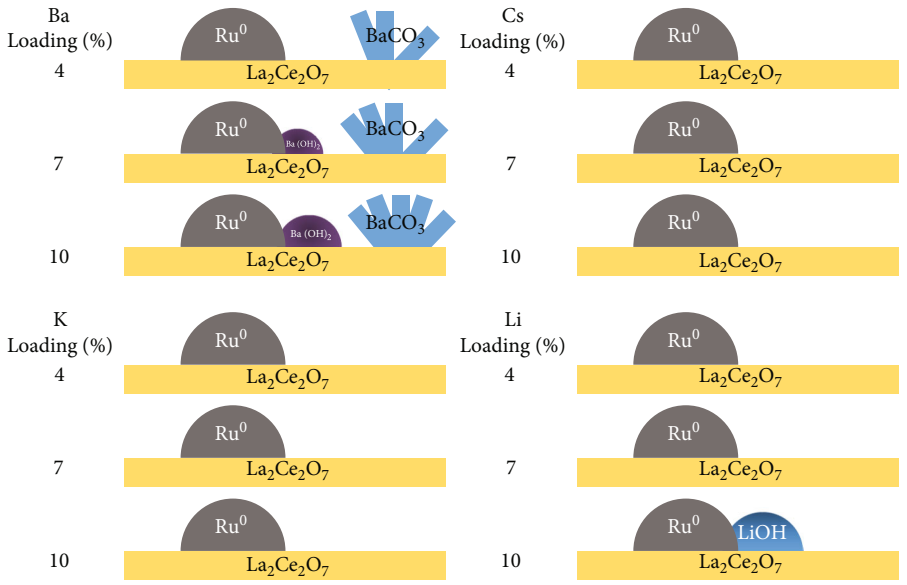

FIGURE 2: The growth of impurities at the Ru/LCO (reduced under 10% H_2/Ar at 450°C for 1 h) surface for different types of promoters.

contribution of the reverse reaction which results in NH_3 concentration way below its thermodynamic equilibrium concentration.

2.3. Characterization. The nanoscale morphology of Ru/LCO catalysts was analyzed by using high-resolution transmission electron microscopy (HRTEM) bright-field imaging, and the distribution of elements was verified through scanning transmission electron microscopy-energy-dispersive X-ray spectroscopy (STEM-EDS) mapping of TEM-Talos. The TEM machine was operated at an accelerating voltage of 200 kV with a magnification of around 1,300,000x. The size of surface Ru particles was determined through the use of ImageJ software.

The SmartLab SE instrument (Rigaku, Tokyo, Japan) was utilized to obtain wide-angle X-ray diffraction (XRD) patterns within the 2θ range of 10-90°. The instrument was set to operate at 30 kV and 20 mA and with a scan speed of 3°/minute. It relied on Cu Kα radiation with a wavelength of 1.54 Å as the X-ray source.

To measure the chemisorption of CO, a 10% CO/He pulsed injection mixture was used with a BELCAT-M catalyst chemisorption analyzer equipped with a thermal conductivity detector (TCD). Prior to the measurements, about 70 mg of catalyst powder that had undergone reduction at 450°C for 1 h under 10% H_2/Ar was subjected to a heating process. This involved heating the powder to 150°C at a rate of 10°C per minute for 30 minutes in 5% H_2/Ar. The reduced powder was then cooled to 50°C before a pulse of CO was charged to initiate CO chemisorption. To calculate the dispersion of Ru metal, CO pulses were repeatedly injected into the tube until there is negligible change in peak area and height for three consecutive peaks. The dispersion was determined by summing up the adsorbed CO and assuming a stoichiometry factor of 1 (Ru : CO = 1 : 1).

A BELCAT-M catalyst chemisorption analyzer was used to conduct temperature-programmed reduction (TPR) and temperature-programmed desorption (TPD) experiments. Prior to the H_2-TPR experiments, around 70 mg of catalyst powder was pretreated with pure Ar gas at 300°C for 1 h to remove any impurities or water from the surface. The temperature was then lowered to 30°C, and the TCD baseline was stabilized before switching to 10% H_2/Ar gas. The temperature was gradually raised to 650°C at a rate of 5°C/min and maintained for 15 minutes. For CO_2-TPD experiment, the samples were pretreated at 500°C for 2 h in pure He gas before exposure with 10% CO_2/He for 1 h. After removing CO_2 and stabilizing the TCD signal by flowing pure He for 1 h, the CO_2 TPD was conducted, and the temperature was gradually raised from 50°C to 900°C at a rate of 10°C/min.

The specific surface areas of the catalysts were determined using the Brunauer-Emmett-Teller (BET) method, which involved pretreating the samples under vacuum at 70°C for 2 h, followed by further degassing at 200°C for approximately 12 h until the pressure dropped below 60-70 mTorr. After cooling down to room temperature, the tube which contains the samples was then transferred to the analysis port to be filled with N_2, and the amount of N_2 adsorbed was measured using a Micromeritics ASAP 2420 instrument. The N_2 adsorption isotherms were measured at a liquid nitrogen temperature of 77 K, with an equilibrium time of 10 seconds.

Elemental composition and chemical states of Ru, La, Ce, O, and promoters in the catalysts were analyzed by X-ray photoelectron spectroscopy (XPS) (K-Alpha+, Thermo Scientific) using monochromatic Al Kα radiation. The carbon 1s binding energy was used as a reference to correct the binding energy. The XPS data was fitted using the XPSPEAK41 software.

3. Results and Discussion

3.1. Structural Analysis. The XRD pattern (Figure 1) revealed the formation of the $La_2Ce_2O_7$ perovskite structure. CeO_2

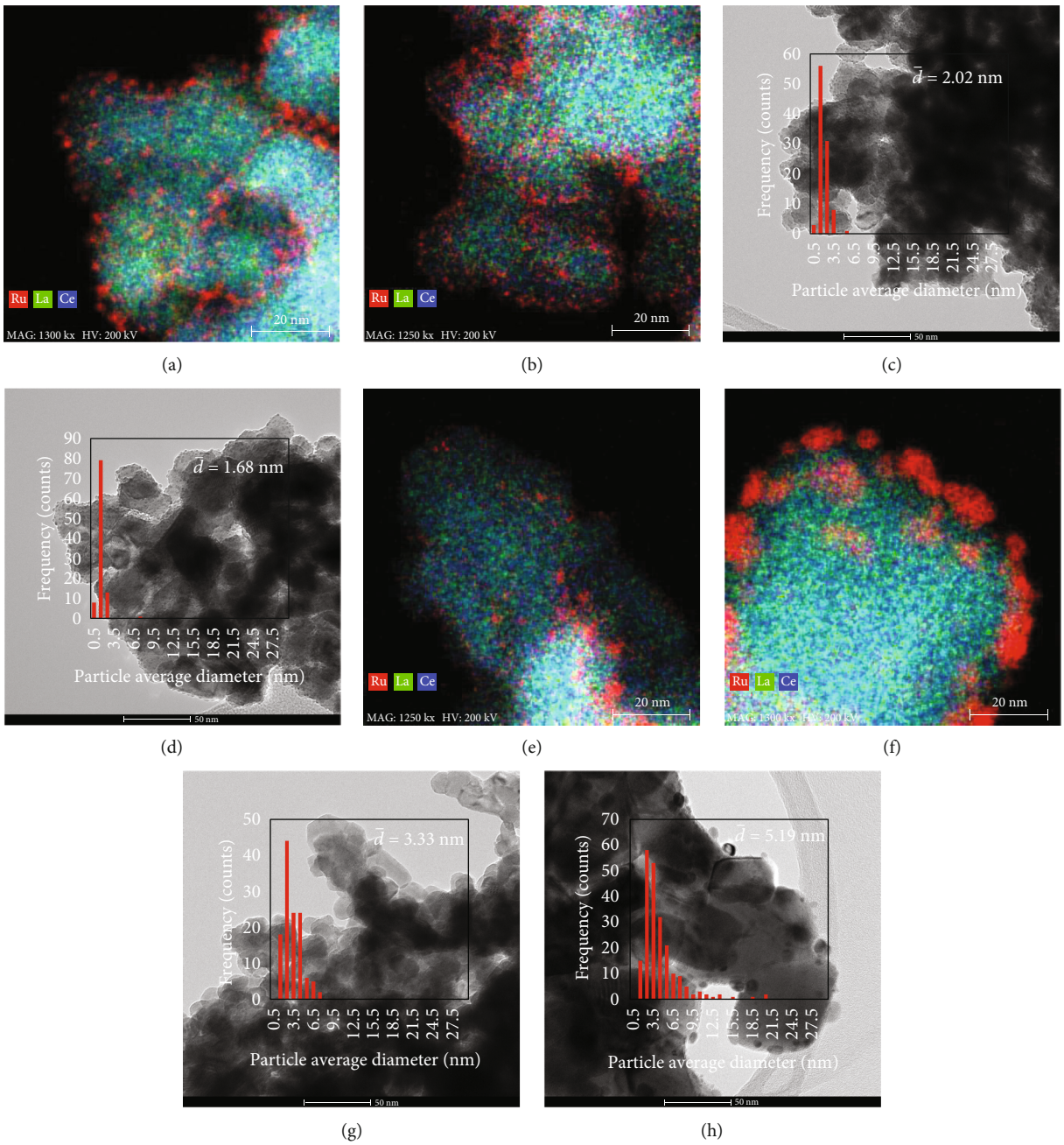

Figure 3: EDS maps of the Ru/LCO catalyst with 4% promoter loading: (a) Ba promoted, (b) Cs promoted, (e) K promoted, (f) and Li promoted after reduction at 450°C for 1 h. STEM images and particle size distribution of the Ru/LCO catalyst with 4% promoter loading: (c) Ba promoted, (d) Cs promoted, (g) K promoted, (h) and Li promoted after reduction at 450°C for 1 h.

and La_2O_3 peaks were unified there and different from the XRD pattern of CeO_2-La_2O_3 composite oxide. Similarly, Ru/LCO peaks were observed by Ogura et al. to be broader and shifted towards lower angles compared to the corresponding peaks for Ru/CeO_2 [5]. XRD patterns were also obtained for promoted Ru/LCO with various promoter loadings (Figures S6–S9). Similar to observations from Sato et al., reduced Ba-promoted catalysts formed more amount of $BaCO_3$ [3]. On the opposite, Cs- and K-promoted Ru/LCO (Figure 2) did not form any kind of impurities, which corresponds well with the XRD peaks of K-promoted Ru/C and Cs-promoted Ru/Al_2O_3 [26, 29]. Based on these results, Cs- and K-promoted Ru/LCO are expected to perform better, owing to no phase impurities in them after promoter loading.

The EDX maps (Figures 3(a), 3(b), 3(e), and 3(f)) of Ru/LCO-promoted catalysts demonstrated the homogeneous dispersion of Ce and La within the oxide support, as well as dispersion of Ru particles on the support. TEM characterization was carried out to investigate the impact of promoter and Ru-promoter interaction on the dispersion of Ru metal. Results depicted in Figures 3(c), 3(d), 3(g), and 3(h) revealed

Table 1: Physicochemical properties and catalytic activities of supported Ru/LCO samples (4 wt% promoter loading).

Catalyst	Promoter	Ru dispersion (%)[a]	NH_3 synthesis rate (mmol g_{cat}^{-1} h^{-1})[b]	SSA[c] (m^2 g^{-1})
Ru/LCO	—	41.9	10.8	53
Ru/4Ba/LCO	Ba	37.6	23.8	38
Ru/4Cs/LCO	Cs	39.1	27.1	11
Ru/4K/LCO	K	22.7	35.9	17
Ru/4Li/LCO	Li	2.1	6.6	6

[a]Determined using CO pulse chemisorption. [b]Measured at 1 MPa, 400°C, and 90 NmL gas flow rate ($H_2/N_2 = 3$). [c]Specific surface area calculated by BET.

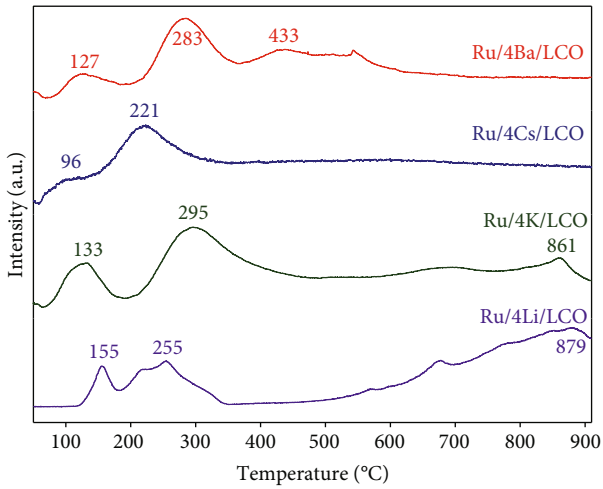

Figure 4: H_2-TPR profiles of the promoted catalyst Ru/LCO.

that the K- and Li-promoted catalysts had larger Ru particles. Statistical analysis indicated that the average size of Ru particles in Ba-, Cs-, K-, and Li-promoted catalysts was 2.02, 1.678, 3.33, and 5.19 nm, respectively. Ideally, the optimum Ru particle size for round particles is around 2.1 nm [30]. The result implies that the interaction between the Ru metal and the promoter induced by various chemical compositions of the support plays a crucial role in stabilizing the size of Ru particles. The size of Ru particles over K- and Li-promoted catalysts is relatively large due to the weak Ru-K and Ru-Li interaction at the interface of Ru-K-LCO and Ru-Li-LCO. Conversely, the reason behind the small size of Ru particles on Ba- and Cs-promoted catalysts is explained by the strong Ru-Ba and Ru-Cs interaction [19]. The large Li-promoted catalyst particle size would in turn affect the catalytic performance severely.

3.2. Physicochemical Analysis. Because the addition of promoters induced the sintering of Ru/LCO and damaged the mesoporous structure of the catalyst, the addition of a nonactive metal to the catalyst is expected to decrease the dispersion and surface area [3, 29]. This is also the case for all catalysts in general. Based on the physicochemical characterization (Table 1), the Ru dispersion of all catalysts decreased with the addition of a promoter. Ba- and Cs-promoted catalysts showed higher Ru dispersion compared to K- and Li-promoted catalysts. This result might be related to the atomic size and molecular weight of the promoters. The order of the promoter's molecular weight is Ba > Cs > K > Li. That means the order of atomic loading is the opposite for the same promoter weight. Aside from each promoter's electronic and structural properties, it seemed reasonable why Li-promoted catalysts showed much lower dispersion and specific surface area because it has much higher atomic loading which covers the Ru and LCO.

However, a study conducted on catalysts consisting of Ru and lanthanoid oxide showed that an increase in the atomic number of the lanthanoid element in the oxide led to a decrease in the specific surface area [28]. Moreover, when we tried to compare 4, 7, and 10 wt% loading for different promoters (Figures S10–S13), the dispersion follows the trend of catalyst NH_3 synthesis rate.

An unexpected result was also obtained from the BET surface area analysis (Figures S14–S17). The surface area of the Ba-promoted catalyst increased when the promoter loading increased from 7 wt% to 10 wt%. The surface area of Cs- and K-promoted catalysts also increased with an increase in the promoter loadings. Unlike the dispersion trends, the BET surface area did not correlate well with catalytic performance. According to Zhou et al., the activity of NH_3 synthesis catalysts cannot be solely determined by the BET surface area [19].

Based on CO chemisorption analysis results, 4 wt% Ba-, 7 wt% Cs-, 4 wt% K-, and 7 wt% Li-promoted catalysts are expected to perform better than the catalysts of other promoter loading levels (Figures S10–S13). At 4 wt% loading, the order of activity of each promoter is expected to be Cs > Ba > K > Li. Similarly, from the BET surface area analysis result, 4 wt% Ba-, 10 wt% Cs-, 10 wt% K-, and 7 wt% Li-loading catalysts are expected to perform better than the catalysts of other promoter loading levels (Figures S14–S18). At 4 wt% promoter loading, the order of activity of each promoter is expected to be Ba > K > Cs > Li.

3.3. Adsorption Analysis. Because of strong metal-support interaction (SMSI), catalysts that can adsorb hydrogen at lower temperatures tend to perform better [31]. There is a hydrogen reduction peak at 127, 96, 133, and 155°C for Ba-, Cs-, K-, and Li-promoted catalysts, respectively (Figure 4). That peak can be attributed to the reduction of RuO_x [32]. Peaks that appear above 200°C are assigned to some RuO_x species that strongly interacted with LCO support or promoter precursors [33]. Based on this analysis, the order of expected performance of each catalyst is Cs > Ba > K > Li. Despite the presence of a peak at 255°C, which

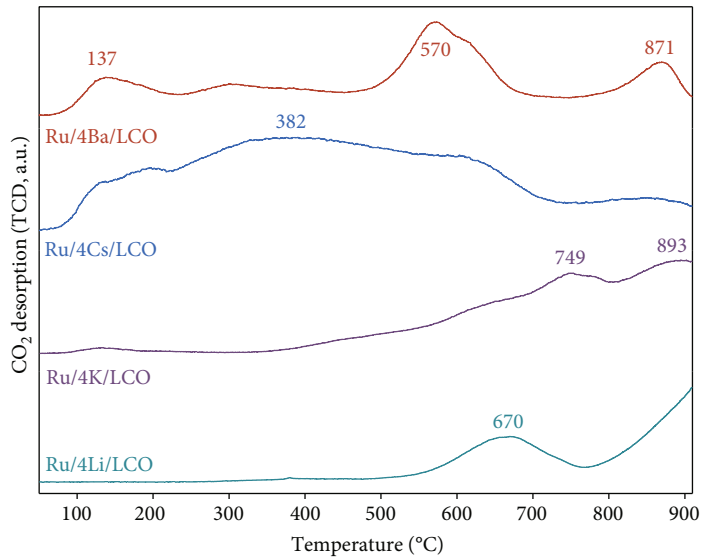

Figure 5: CO_2-TPD desorption profiles of Ru/P/LCO (P = Ba, Cs, K, Li, Li-Ba).

is lower than that of K at 295°C, the Ru/4Li/LCO H_2-TPR result has a more dominant peak at temperatures higher than 650°C, which can be assigned to the reduction of the support material.

Catalysts with higher basicity are more desirable for ammonia synthesis [34–37]. In general, the activity of a catalyst is decreased by the presence of acidic sites due to their ability to withdraw electrons. Strong basicity, on the other hand, has been shown to be a crucial factor for achieving high activity. This is because strong basic sites can transfer their electrons to the surface of Ru particles, which promotes the recombinative desorption of N atoms [38]. The basicity of the promoter solution also alters the mesoporous structure of the catalyst [39]. Figure 5 shows the basicity, as determined by CO_2-TPD. The desorption peaks below 250°C indicate the presence of weak basic sites, while those between 250°C and 500°C represent moderate basic sites [40, 41]. Furthermore, the peaks observed at temperatures exceeding 500°C can be attributed to the existence of highly basic sites. Strong basic sites were observed in all the promoter catalysts except Ru/Cs/$La_2Ce_2O_7$, which also has two weak basic sites. This result was not in accordance with Ru/Cs-MgO catalysts which showed superbasic sites that showed a desorption peak at 640°C [42].

3.4. Electronic State Analysis. The N_2 dissociation ability of the catalyst is strongly linked to the electronic configuration of the Ru sites. Specifically, the XPS spectra of Ru 3d in Figure 6(a) show three peaks corresponding to RuO_2, RuO_3, and Ru^0, located at 281.1, 282.5, and 279.7 eV, respectively [43–45]. Contents of various Ru, Cs, and O species for Ru/LCO samples are shown in Table 2. The addition of a promoter promotes the formation of metallic Ru, but the Li-promoted catalyst stands out from the rest with 31.6% of Ru^0 contents. Considering the overlap between C 1s and Ru $3d_{3/2}$ peaks, the Ru 3p profiles were also analyzed (Figure 6(b)). The Ba-, Cs-, and K-promoted catalysts showed a Ru $3p_{3/2}$ peak within the range of 462.62-462.81 eV, while the Li-promoted catalyst had a peak at 461.62 eV, indicating a weaker interaction between the Ru atoms and LCO [46]. In Figure 6(c), it can be seen that all La 3d spectral curves showed wide doublet peaks. Compared with Ru/LCO, the addition of promoters decreases the La $3d_{5/2}$ binding energy and creates a rich electron surface except for the Cs-promoted catalyst.

Figure 6(d) illustrates the Ce 3d XPS regions that have been deconvoluted for all the samples of Ru/LCO. A pair of $3d_{5/2}$ (880.5 and 884.9 eV) is assigned to Ce^{3+}, and the other pair (882.1 and 884.6 eV) is assigned to Ce^{4+}. The other pairs are ascribed to Ce $3d_{3/2}$ species. There was supposed to be a pair of $3d_{3/2}$ peaks (898.9 and 903.3 eV) which are assigned to Ce^{3+}, but we hardly observed it. The percentage of Ce^{3+} in the total Ce contents is 31.2% for Ru/Ba/LCO, indicating that the addition of Ba increased the Ce^{3+} concentration and oxygen vacancies [47]. The O 1s XPS spectra (Figure 6(e)) contain a peak at around 531.4 eV binding energy, which is assumed to be caused by oxygen species adsorbed on the surface (referred to as O_{ads}). Another peak observed at 529.3 eV is believed to be caused by lattice oxygen (referred to as O_{latt}) of RuO_3 and/or LCO. The O_{latt} content was affected by the strong metal-support interaction effect (SMSI), reduction methods, and Ru, La, and Ce oxidation states [48]. Table 2 showed that the addition of promoters to Ru/LCO increases the concentration of surface-adsorbed oxygen. The most significant increase was observed in the Li-promoted catalyst. The XPS results showed that each promoter affects Ru, Ce, La, and O differently in terms of electronic properties.

In Ba-promoted catalysts, the increase in promoter loading increased the oxidation state of La, Ru 3p, and Ba 3d and increased the amount of O_{ads}. However, some irregularities were observed in Ce 3d and Ru 3d scanning, with 7 wt% Ba loading and 10 wt% Ba loading having the least amount of Ce^{3+} and the highest amount of Ru^0, respectively

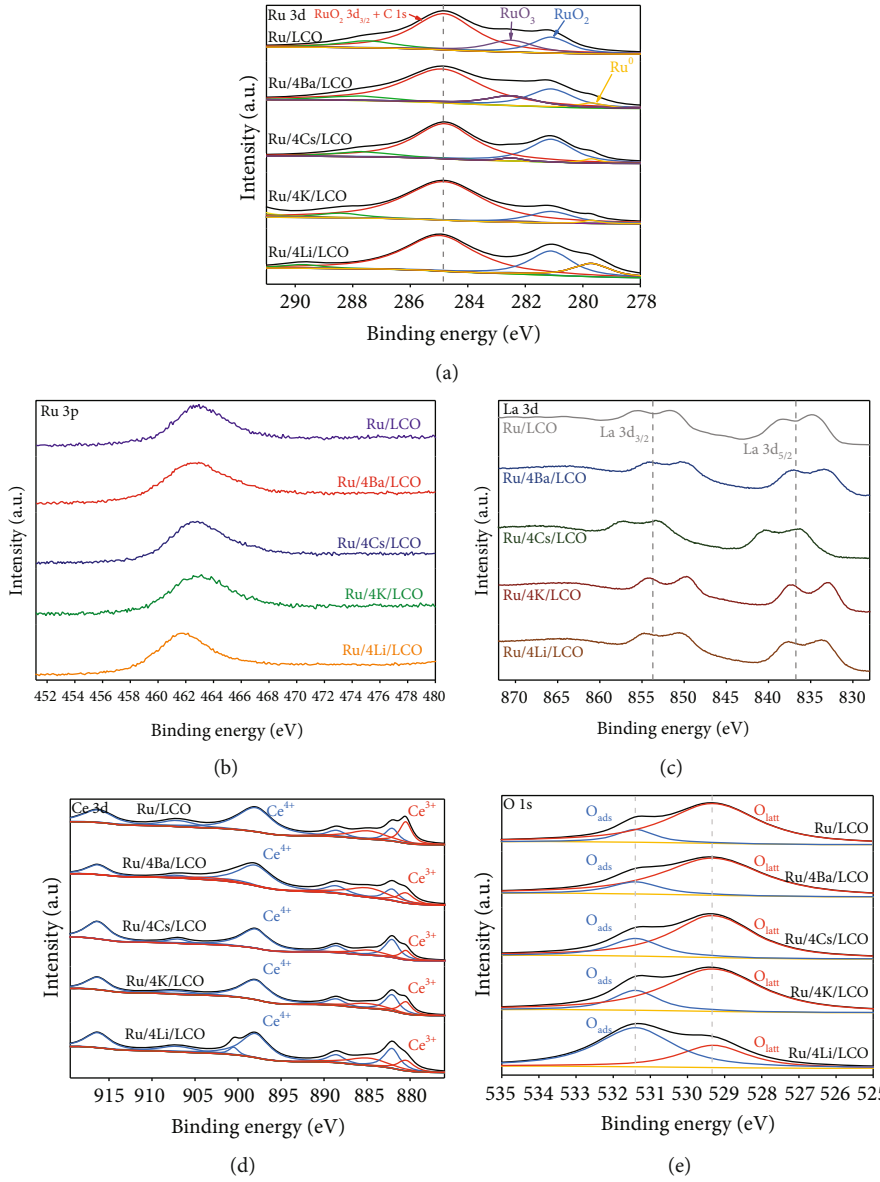

Figure 6: (a) Ru 3d, (b) Ru 3p, (c) La 3d, (d) Ce 3d, and (e) O 1s XPS spectra.

Table 2: XPS spectra fitting results of Ru 3d, Ce 3d, and O 1s for different Ru/LCO samples.

Catalyst name	Promoter	$Ru^0/(Ru^0 + Ru^{n+})$	$Ce^{3+}/(Ce^{3+} + Ce^{4+})$	$O_{ads}/(O_{ads} + O_{latt})$
Ru/LCO	—	0	24.3%	11.6%
Ru/4Ba/LCO	Ba	9.7%	31.2%	13.6%
Ru/4Cs/LCO	Cs	6.9%	17.6%	20.1%
Ru/4K/LCO	K	8.4%	19.1%	18.0%
Ru/4Li/LCO	Li	31.6%	20.7%	66.1%

(Figure S18). Among the Cs-promoted catalysts, the 4 wt% Cs catalyst had the highest amounts of Ce^{3+}, Ru^0, and O_{latt} and the lowest oxidation states of Ru 3p and Cs 3d. However, some irregularities were observed in all the scanned components, and the addition of Cs loading did not necessarily increase their corresponding oxidation state (Figure S19). In the K-promoted catalysts, the 7 wt% K-loaded catalyst had the highest amounts of Ce^{3+}, Ru^0, and O_{latt} and the lowest oxidation state for La 3d and Ru 3p and is therefore expected to perform better than the others (Figure S20). In the Li-promoted catalysts, an increase in the promoter loading increased the oxidation states of La, Ru, and Li and decreased the amounts of Ce^{3+} and O_{latt}. Based on this result, a loading level of 4 wt% is expected to

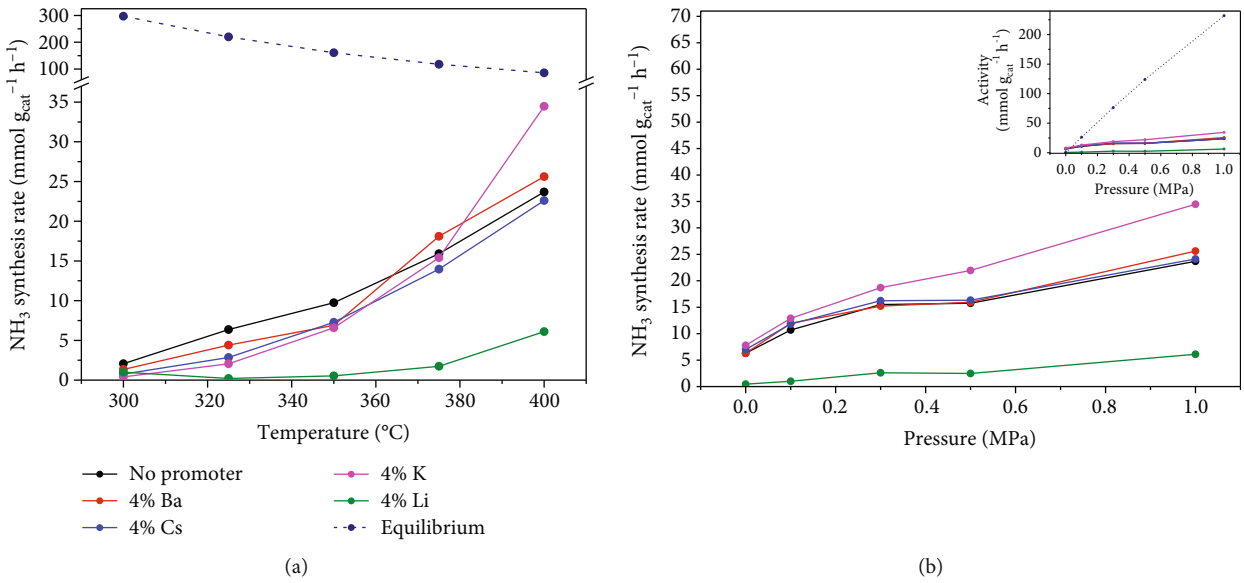

Figure 7: Catalytic activity test: (a) effect of temperature of the ammonia synthesis rate at 1 MPa; (b) effect of temperature of the ammonia synthesis rate at 400°C; each catalyst had been reduced at 450°C.

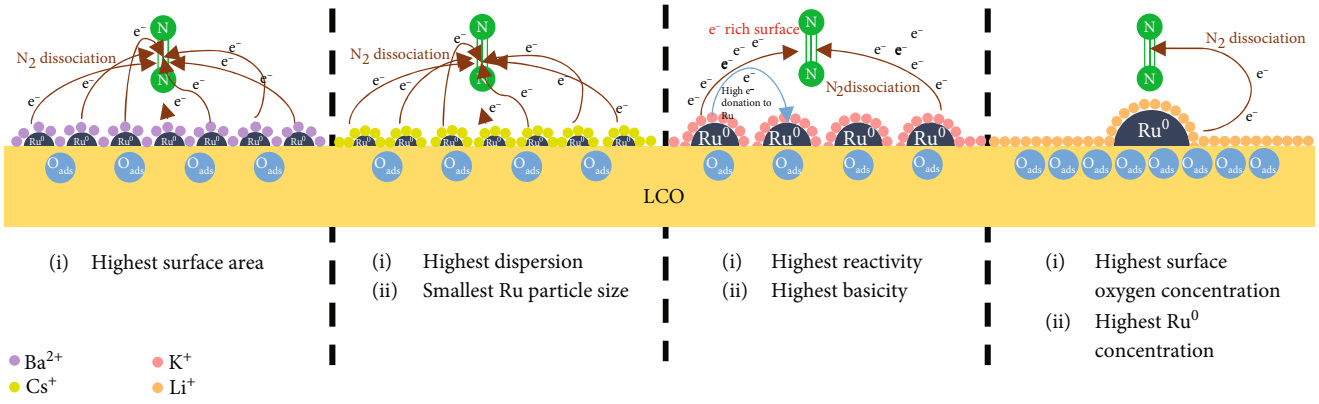

Figure 8: Schematic graph summarizing the promoter effect of Ru/LCO catalysts.

have the best performance (Figure S21). Generally, the addition of a promoter increases the oxidation state of each catalyst component; however, some irregularities were also observed.

3.5. Performance Test. Based on Figure 7, the performance of the catalysts was evaluated. The extent of reproducibility of activity measurement is visualized in Figures S24–S28. Overall, the reaction test showed that the catalyst activity values still fell below the equilibrium value. The activity test suggested the catalyst activity order for each promoter to be K > Cs > Ba > Li at 400°C and 1 MPa which also showed how fast the reaction reached the equilibrium (Figure 7(a)). It is clearly seen that Li addition greatly decreased the Ru/LCO activity, but the addition of Li can be beneficial if we use the right amount (Figure S5). One of the reasons for such an anomaly is that Li has very low atomic mass which means, as we have discussed in the physicochemical testing part, there are a lot more Li atoms covering Ru and LCO surfaces compared to other promoters. Ba-promoted Ru/LCO has been tested before by Sato et al., yet we still tested that catalyst in order to find where it stands compared to our other samples [3]. The pressure dependence result of the catalyst activity test showed a decrease in the Ba-promoted catalyst with the increase in temperature (Figure 7(b)). In terms of optimal composition, 4 wt% Ba, 7 wt% Cs, 4 wt% K, and 7 wt% Li were observed to exhibit the best performance for each type of promoter (Figures S2–S5). It is also worth noticing that some catalysts were still active at 0 MPa like electrochemical cells do [49]. In fuel cells, reaction at 0 MPa is enabled by the presence of a proton conductor (H^+). This might also be the case in this study where our catalysts assisted not only N_2 but also H_2 dissociation. The K-promoted catalyst had the highest catalytic performance due to its very high basicity observed on CO_2-TPD. On the other hand, despite also having a high basicity and high surface oxygen concentration, the Li-promoted catalyst still obtains a low activity due to their low Ru dispersion. Therefore, it has a low ability to dissociate N_2.

The pressure dependence test indicated that the rate of ammonia synthesis increased (not proportionally) with Cs-, K-, and Li-promoted catalysts, and not with Ba-promoted catalysts. The Ba-promoted catalyst could be more prone to H_2 poisoning, a phenomenon in which H_2 is strongly bonded to Ru active sites at higher pressure, blocking the main reaction [10]. Sabatier's principle suggests that the most efficient catalysts are those that bind atoms and molecules with optimal strength. If the binding is too weak, the catalysts will not be able to retain the reactants on their surface, resulting in no reaction. On the other hand, if the binding is too strong, the catalysts will not be able to release the products, which reduces the catalyst activity [50].

4. Conclusions

To increase the reactivity of Ru/LCO catalysts for thermochemical ammonia synthesis, several promoters have been added, and their effect on the morphological and chemical characteristics of the catalysts was experimentally studied in detail. The highlight of our research is illustrated in Figure 8, and the summary of our findings is as the following: Ru/LCO can maintain its structural properties and minimize phase impurities with the addition of promoters. The order of reactivity of promoted Ru/LCO in this study is K > Cs > Ba > Li. Some promoters are also able to increase the catalytic performance despite decreasing the catalyst surface area and Ru dispersion. The atomic mass of each promoter played a key part there. Despite having the second-highest atomic mass among the other promoters, the addition of the K promoter displayed the highest effectiveness for Ru/LCO compared with other promoters used in this study because of its phase purity and very high basicity. It increases the reaction rate by 3 times compared with Ru/LCO and 1.5 times compared with the developed Ru/Ba/LCO. Despite poor performance at lower-pressure synthesis, the Ba promoter can perform well under mild conditions, such as in fuel cells. These findings are important for the development of Ru/LCO-based catalysts for hydrogen storage/production.

Data Availability

The original data can be obtained upon request, and additional supporting information can be found online in the supporting information section located at the end of the article.

Conflicts of Interest

The authors of this manuscript declare that there are no competing interests.

Authors' Contributions

Hizkia Manuel Vieri and Arash Badakhsh have contributed equally to this work.

Acknowledgments

This work was supported by the National Research Foundation Grant funded by the Korean Government (Ministry of ICT) (Grant No. 2021R1A2C2008662).

Supplementary Materials

Figure S1: reduction temperature optimization. Figure S2: catalytic activity test of Ru/Ba/LCO with different promoter loading: (a) pressure dependence of the ammonia synthesis rate at 400°C; (b) temperature dependence of the ammonia synthesis rate at 1 MPa, each of which had been reduced at 450°C. Figure S3: catalytic activity test of Ru/Cs/LCO with different promoter loading: (a) pressure dependence of the ammonia synthesis rate at 400°C; (b) temperature dependence of the ammonia synthesis rate at 1 MPa, each of which had been reduced at 450°C. Figure S4: catalytic activity test of Ru/K/LCO with different promoter loading: (a) pressure dependence of the ammonia synthesis rate at 400°C; (b) temperature dependence of the ammonia synthesis rate at 1 MPa, each of which had been reduced at 450°C. Figure S5: catalytic activity test of Ru/K/LCO with different promoter loading: (a) pressure dependence of the ammonia synthesis rate at 400°C; (b) temperature dependence of the ammonia synthesis rate at 1 MPa, each of which had been reduced at 450°C. Figure S6: X-ray diffraction patterns of Ru/Ba/LCO with different promoter compositions. Figure S7: X-ray diffraction patterns of Ru/Cs/LCO with different promoter compositions. Figure S8: X-ray diffraction patterns of Ru/K/LCO with different promoter compositions. Figure S9: X-ray diffraction patterns of Ru/Li/LCO with different promoter compositions. Figure S10: NH_3 synthesis rate correlation with Ru dispersion for Ru/Ba/LCO. Figure S11: NH_3 synthesis rate correlation with Ru dispersion for Ru/Cs/LCO. Figure S12: NH_3 synthesis rate correlation with Ru dispersion for Ru/K/LCO. Figure S13: NH_3 synthesis rate correlation with Ru dispersion for Ru/Li/LCO. Figure S14: NH_3 synthesis rate correlation with BET surface area for Ru/Ba/LCO. Figure S15: NH_3 synthesis rate correlation with BET surface area for Ru/Cs/LCO. Figure S16: NH_3 synthesis rate correlation with BET surface area for Ru/K/LCO. Figure S17: NH_3 synthesis rate correlation with BET surface area for Ru/Li/LCO. Figure S18: XPS spectra of Ru/Ba/LCO with different promoter loading. Figure S19: XPS spectra of Ru/Cs/LCO with different promoter loading. Figure S20: XPS spectra of Ru/K/LCO with different promoter loading. Figure S21: XPS spectra of Ru/Li/LCO with different promoter loading. Figure S22: H_2SO_4 conductivity value when measuring NH_3 synthesis rate at 400°C and 0.5 MPa. Figure S23: H_2SO_4 conductivity value when calibrated using NH_3 solution. Figure S24: reproducibility proof of Ru/LCO catalyst: (a) temperature dependence of the ammonia synthesis rate at 1 MPa; (b) pressure dependence of the ammonia synthesis rate at 400°C; each catalyst had been reduced at 450°C. Figure S25: reproducibility proof of Ru/Ba/LCO catalyst: (a) temperature dependence of the ammonia synthesis rate at 1 MPa; (b) pressure dependence of the ammonia synthesis rate at 400°C; each catalyst had been reduced at 450°C.

Figure S26: reproducibility proof of Ru/Cs/LCO catalyst: (a) temperature dependence of the ammonia synthesis rate at 1 MPa; (b) pressure dependence of the ammonia synthesis rate at 400°C; each catalyst had been reduced at 450°C. Figure S27: reproducibility proof of Ru/K/LCO catalyst: (a) temperature dependence of the ammonia synthesis rate at 1 MPa; (b) pressure dependence of the ammonia synthesis rate at 400°C; each catalyst had been reduced at 450°C. Figure S28: reproducibility proof of Ru/Li/LCO catalyst: (a) temperature dependence of the ammonia synthesis rate at 1 MPa; (b) pressure dependence of the ammonia synthesis rate at 400°C; each catalyst had been reduced at 450°C. *(Supplementary Materials)*

References

[1] D. Teichmann, K. Stark, K. Müller, G. Zöttl, P. Wasserscheid, and W. Arlt, "Energy storage in residential and commercial buildings via Liquid Organic Hydrogen Carriers (LOHC)," *Energy and Environmental Science*, vol. 5, no. 10, pp. 9044–9054, 2012.

[2] T. Kandemir, M. E. Schuster, A. Senyshyn, M. Behrens, and R. Schlögl, "The Haber-Bosch process revisited: on the real structure and stability of "ammonia iron" under working conditions," *Angewandte Chemie International Edition*, vol. 52, no. 48, pp. 12723–12726, 2013.

[3] K. Sato, S. Miyahara, Y. Ogura et al., "Surface dynamics for creating highly active ru sites for ammonia synthesis: accumulation of a low-crystalline, oxygen-deficient nanofraction," *ACS Sustainable Chemistry & Engineering*, vol. 8, no. 7, pp. 2726–2734, 2020.

[4] K. I. Aika, H. Hori, and A. Ozaki, "Activation of nitrogen by alkali metal promoted transition metal I. Ammonia synthesis over ruthenium promoted by alkali metal," *Journal of Catalysis*, vol. 27, no. 3, pp. 424–431, 1972.

[5] Y. Ogura, K. Sato, S. Miyahara et al., "Efficient ammonia synthesis over a $Ru/La_{0.5}Ce_{0.5}O_{1.75}$ catalyst pre-reduced at high temperature," *Chemical Science*, vol. 9, no. 8, pp. 2230–2237, 2018.

[6] J. Humphreys, R. Lan, S. Chen, M. Walker, Y. Han, and S. Tao, "Cation doped cerium oxynitride with anion vacancies for Fe-based catalyst with improved activity and oxygenate tolerance for efficient synthesis of ammonia," *Applied Catalysis B: Environmental*, vol. 285, article 119843, 2021.

[7] C. Li, Z. Zhang, Y. Zheng et al., "Titanium modified Ru/CeO_2 catalysts for ammonia synthesis," *Chemical Engineering Science*, vol. 251, article 117434, 2022.

[8] C. Li, Z. Zhang, Y. Zheng et al., "Enhancement of ammonia synthesis activity on La_2O_3-supported Ru catalyst by addition of ceria," *International Journal of Hydrogen Energy*, vol. 47, no. 55, pp. 23240–23248, 2022.

[9] S. E. Siporin, B. C. McClaine, S. L. Anderson, and R. J. Davis, "Lanthanum promotion of Ru/zeolite X catalysts for ammonia synthesis," *Catalysis Letters*, vol. 81, no. 3/4, pp. 265–269, 2002.

[10] Y. Kadowaki and K. I. Aika, "Promoter effect of Sm_2O_3on Ru/Al_2O_3in ammonia synthesis," *Journal of Catalysis*, vol. 161, no. 1, pp. 178–185, 1996.

[11] K. Aika, K. Shimazaki, Y. Hattori et al., "Support and promoter effect of ruthenium catalyst: I. Characterization of alkali-promoted ruthenium/alumina catalysts for ammonia synthesis," *Journal of Catalysis*, vol. 92, no. 2, pp. 296–304, 1985.

[12] W. Gao, P. Wang, J. Guo et al., "Barium hydride-mediated nitrogen transfer and hydrogenation for ammonia synthesis: a case study of cobalt," *ACS Catalysis*, vol. 7, no. 5, pp. 3654–3661, 2017.

[13] B. Lin, K. Wei, X. Ma, J. Lin, and J. Ni, "Study of potassium promoter effect for Ru/AC catalysts for ammonia synthesis," *Catalysis Science and Technology*, vol. 3, no. 5, pp. 1367–1374, 2013.

[14] K. Aika, "Role of alkali promoter in ammonia synthesis over ruthenium catalysts–effect on reaction mechanism," *Catalysis Today*, vol. 286, pp. 14–20, 2017.

[15] J. Zheng, F. Liao, S. Wu et al., "Efficient non-dissociative activation of dinitrogen to ammonia over lithium- promoted ruthenium nanoparticles at low pressure," *Angewandte Chemie International Edition*, vol. 58, no. 48, pp. 17335–17341, 2019.

[16] C. J. H. Jacobsen, "Boron nitride: a novel support for ruthenium-based ammonia synthesis catalysts," *Journal of Catalysis*, vol. 200, no. 1, pp. 1–3, 2001.

[17] Y. V. Larichev, B. L. Moroz, V. I. Zaikovskii et al., "XPS and TEM studies on the role of the support and alkali promoter in Ru/MgO and $Ru–Cs^+/MgO$ catalysts for ammonia synthesis," *Journal of Physical Chemistry C*, vol. 111, no. 26, pp. 9427–9436, 2007.

[18] G. P. Connor and P. L. Holland, "Coordination chemistry insights into the role of alkali metal promoters in dinitrogen reduction," *Catalysis Today*, vol. 286, pp. 21–40, 2017.

[19] Y. Zhou, X. Peng, T. Zhang et al., "Essential role of Ru–anion interaction in Ru-based ammonia synthesis catalysts," *ACS Catalysis*, vol. 12, no. 13, pp. 7633–7642, 2022.

[20] C. J. H. Jacobsen, S. Dahl, P. L. Hansen et al., "Structure sensitivity of supported ruthenium catalysts for ammonia synthesis," *Journal of Molecular Catalysis A: Chemical*, vol. 163, no. 1-2, pp. 19–26, 2000.

[21] H. Bielawa, O. Hinrichsen, A. Birkner, and M. Muhler, "The ammonia-synthesis catalyst of the next generation: barium-promoted oxide-supported ruthenium," *Angewandte Chemie International Edition*, vol. 40, no. 6, pp. 1061–1063, 2001.

[22] W. Raróg, Z. Kowalczyk, J. Sentek, D. Składanowski, and J. Zieliński, "Effect of K, Cs and Ba on the kinetics of NH_3 synthesis over carbon-based ruthenium catalysts," *Catalysis Letters*, vol. 68, no. 3/4, pp. 163–168, 2000.

[23] L. Forni, D. Molinari, I. Rossetti, and N. Pernicone, "Carbon-supported promoted Ru catalyst for ammonia synthesis," *Applied Catalysis A: General*, vol. 185, no. 2, pp. 269–275, 1999.

[24] W. Li, S. Wang, and J. Li, "Highly effective $Ru/BaCeO_3$ catalysts on supports with strong basic sites for ammonia synthesis," *Chemistry, an Asian Journal*, vol. 14, pp. 2815–2821, 2019.

[25] B. Lin, Y. Qi, Y. Guo, J. Lin, and J. Ni, "Effect of potassium precursors on the thermal stability of K-promoted Ru/carbon catalysts for ammonia synthesis," *Catalysis Science & Technology*, vol. 5, no. 5, pp. 2829–2838, 2015.

[26] Z. Kowalczyk, S. Jodzis, W. Raróg, J. Zieliński, and J. Pielaszek, "Effect of potassium and barium on the stability of a carbon-supported ruthenium catalyst for the synthesis of ammonia," *Applied Catalysis A: General*, vol. 173, no. 2, pp. 153–160, 1998.

[27] A. Badakhsh, H. M. Vieri, H. Sohn, S. P. Yoon, and S. H. Choi, "Exsolved Ru on $BaCe_xO_y$ catalysts for thermochemical

ammonia synthesis," *International Journal of Energy Research*, vol. 2023, article 9919748, 14 pages, 2023.

[28] S. Miyahara, K. Sato, Y. Kawano et al., "Ammonia synthesis over lanthanoid oxide-supported ruthenium catalysts," *Catalysis Today*, vol. 376, pp. 36–40, 2021.

[29] B. J. Kim, D. F. Abbott, X. Cheng et al., "Unraveling thermodynamics, stability, and oxygen evolution activity of strontium ruthenium perovskite oxide," *ACS Catalysis*, vol. 7, no. 5, pp. 3245–3256, 2017.

[30] B. Lin, K. Wei, J. Lin, and J. Ni, "Effect of treatment conditions on ruthenium particle size and ammonia synthesis activity of ruthenium catalyst," *Catalysis Communications*, vol. 39, pp. 14–19, 2013.

[31] Y. Manaka, Y. Nagata, K. Kobayashi, D. Kobayashi, and T. Nanba, "The effect of a ruthenium precursor on the low-temperature ammonia synthesis activity over Ru/CeO_2," *Dalton Transactions*, vol. 49, no. 47, pp. 17143–17146, 2020.

[32] J. Feng, L. Liu, X. Zhang et al., "Ru nanoparticles on Y_2O_3 with enhanced metal–support interactions for efficient ammonia synthesis," *Catalysis Science & Technology*, vol. 2, pp. 636–639, 2022.

[33] B. Lin, B. Fang, Y. Wu et al., "Enhanced ammonia synthesis activity of ceria-supported ruthenium catalysts induced by CO activation," *ACS Catalysis*, vol. 11, no. 3, pp. 1331–1339, 2021.

[34] S. F. Yin, B. Q. Xu, C. F. Ng, and C. T. Au, "Nano Ru/CNTs: a highly active and stable catalyst for the generation of CO_x-free hydrogen in ammonia decomposition," *Applied Catalysis B: Environmental*, vol. 48, no. 4, pp. 237–241, 2004.

[35] S. J. Wang, S. F. Yin, L. Li, B. Q. Xu, C. F. Ng, and C. T. Au, "Investigation on modification of Ru/CNTs catalyst for the generation of CO_x-free hydrogen from ammonia," *Applied Catalysis B: Environmental*, vol. 52, no. 4, pp. 287–299, 2004.

[36] A. K. Hill and L. Torrente-Murciano, "Low temperature H_2 production from ammonia using ruthenium-based catalysts: synergetic effect of promoter and support," *Applied Catalysis B: Environmental*, vol. 172-173, pp. 129–135, 2015.

[37] S. F. Yin, B. Q. Xu, S. J. Wang, C. F. Ng, and C. T. Au, "Magnesia–carbon nanotubes (MgO–CNTs) nanocomposite: novel support of Ru catalyst for the generation of CO_x-free hydrogen from ammonia," *Catalysis Letters*, vol. 96, no. 3/4, pp. 113–116, 2004.

[38] Z. Wang, Z. Cai, and Z. Wei, "Highly active ruthenium catalyst supported on barium exaaluminate for ammonia decomposition to CO_x-free hydrogen," *ACS Sustainable Chemical Engineering*, vol. 7, no. 9, pp. 8226–8235, 2019.

[39] M. J. Banisalman, M.-C. Kim, and S. S. Han, "Origin of enhanced ammonia synthesis on Ru–Co catalysts unraveled by density functional theory," *ACS Catalysis*, vol. 12, no. 2, pp. 1090–1097, 2022.

[40] X. Zhu, X. Hu, X. Wu, Y. Cai, H. Zhang, and X. Tu, "Ammonia synthesis overγ-Al_2O_3 pellets in a packed-bed dielectric barrier discharge reactor," *Journal of Physics D: Applied Physics*, vol. 53, no. 16, article 164002, 2020.

[41] Z. Wang, B. Liu, and J. Lin, "Highly effective perovskite-type $BaZrO_3$ supported Ru catalyst for ammonia synthesis," *Applied Catalysis A: General*, vol. 458, pp. 130–136, 2013.

[42] L. Liu, X. Zhang, X. Ju, J. Feng, J. Wang, and P. Chen, "Ru nanoparticles on a Cs-loaded MgO superbase as highly efficient catalysts for ammonia synthesis," *Dalton Transactions*, vol. 50, no. 35, pp. 12074–12078, 2021.

[43] H. Huang, Q. Dai, and X. Wang, "Morphology effect of Ru/CeO_2 catalysts for the catalytic combustion of chlorobenzene," *Applied Catalysis B: Environmental*, vol. 158-159, pp. 96–105, 2014.

[44] C. Elmasides, D. I. Kondarides, W. Grünert, and X. E. Verykios, "XPS and FTIR study of Ru/Al_2O_3 and Ru/TiO_2 catalysts: reduction characteristics and interaction with a methane–oxygen mixture," *Journal of Physical Chemistry B*, vol. 103, no. 25, pp. 5227–5239, 1999.

[45] B. Lin, Y. Liu, L. Heng et al., "Morphology effect of ceria on the catalytic performances of Ru/CeO_2catalysts for ammonia synthesis," *Industrial & Engineering Chemistry Research*, vol. 57, no. 28, pp. 9127–9135, 2018.

[46] S. Ahn, K. Park, K. R. Lee et al., "Atomically dispersed Ru(III) on N-doped mesoporous carbon hollow spheres as catalysts for CO_2 hydrogenation to formate," *Chemical Engineering Journal*, vol. 442, article 136185, 2022.

[47] C. Li, Y. Shi, Z. Zhang et al., "Improving the ammonia synthesis activity of Ru/CeO_2 through enhancement of the metal-support interaction," *Journal of Energy Chemistry*, vol. 60, pp. 403–409, 2021.

[48] X. Wang, X. Peng, H. Ran, B. Lin, J. Ni, and L. Jiang, "Influence of Ru substitution on the properties of $LaCoO_3$ Catalysts for ammonia synthesis: XAFS and XPS studies," *Industrial & Engineering Chemistry Research*, vol. 57, no. 51, pp. 17375–17383, 2018.

[49] G. Marnellos and M. Stoukides, "Ammonia synthesis at atmospheric pressure," *Science*, vol. 282, no. 5386, pp. 98–100, 1998.

[50] A. J. Medford, A. Vojvodic, J. S. Hummelshøj et al., "From the Sabatier principle to a predictive theory of transition-metal heterogeneous catalysis," *Journal of Catalysis*, vol. 328, pp. 36–42, 2015.